CHEMICAL PHYSICS

Survival of spin state in magnetic porphyrins contacted by graphene nanoribbons

Jingcheng Li,[1,2]* Nestor Merino-Díez,[1,3] Eduard Carbonell-Sanromà,[1] Manuel Vilas-Varela,[4] Dimas G. de Oteyza,[2,3,5] Diego Peña,[4] Martina Corso,[2,3] Jose Ignacio Pascual[1,5]*

We report on the construction and magnetic characterization of a fully functional hybrid molecular system composed of a single magnetic porphyrin molecule bonded to graphene nanoribbons with atomically precise contacts. We use on-surface synthesis to direct the hybrid creation by combining two molecular precursors on a gold surface. High-resolution imaging with a scanning tunneling microscope finds that the porphyrin core fuses into the graphene nanoribbons through the formation of new carbon rings at chemically predefined positions. These ensure the stability of the hybrid and the extension of the conjugated character of the ribbon into the molecule. By means of inelastic tunneling spectroscopy, we prove the survival of the magnetic functionality of the contacted porphyrin. The molecular spin appears unaffected by the graphenoid electrodes, and we simply observe that the magnetic anisotropy appears modified depending on the precise structure of the contacts.

INTRODUCTION

Wiring single molecules into electronic circuits requires atomically precise control of their connection to the electrodes. The use of metal electrodes is usually hampered by the lack of well-defined molecule-electrode contacts with high transparency and reproducibility (*1*). Graphene and graphene nanoribbons (GNRs) are ideal systems for contacting functional molecules (*2*, *3*) due to their extraordinary electron mobility and structural stability under high currents (*4*). Robust molecular devices can be made with C–C covalent bonds connecting a molecule to graphene electrodes (*5*–*7*) under the premise that the functionality of molecules is not affected. Thus, synthetic strategies to produce covalent junctions with a predefined shape are crucial.

Atomically precise GNRs can be produced by surface-assisted polymerization and subsequent cyclodehydrogenation (CDH) of molecular precursors on a metal surface (*8*–*11*). By combining different building blocks, hybrid GNR structures with potential functionality, such as heterojunctions (*12*, *13*) or quantum dots (*14*), have been produced. Using a similarly precise and selective on-surface synthesis strategy, we aimed at covalently connecting GNRs to a porphyrin molecule. Ideally, this molecular-scale device would use the functionality of porphyrin units as magnetic (*15*, *16*) or optically (*17*) active elements, whereas the GNR segments would electrically address the function by transporting electron currents to source/drain electrodes. Ultimately, the resulting molecular system should maintain the functionality of the components unaffected by their interconnection.

Here, we study nanoscale magnetic system fabricated following the process illustrated in Fig. 1 (A to C). Two types of molecular building blocks are combined. To create the connecting GNR leads, we used 2,2′-dibromo-9,9′-bianthracene (DBBA) (Fig. 1A). This monomer has been reported (*10*) to form chiral GNRs (cGNRs) with edges alternating zigzag and armchair units in a three to one sequence [that is, (3,1) cGNRs]. The CDH temperature of these ribbons ($T \sim 475$ K) is relatively low, which reduces the probability of forming by-products. As an active element, we chose Fe-tetra(4-bromophenyl)porphyrin chloride [Br_4-FeTPP(Cl)] (Fig. 1A). The Fe ion in the center endows the molecular component with a well-known magnetic ground state (*15*, *16*). At temperatures slightly above the room temperature, the Cl ligand is detached, and the oxidation state of the iron ion changes from Fe^{3+} to Fe^{2+} (*18*). This leaves the Fe-tetraphenyl-porphyrin (FeTPP) core in an $S = 1$ magnetic state. The four Br atoms at the para-phenyl position mediate the covalent connection between FeTPP and GNR via C–C Ullmann coupling reactions (*19*), resulting in the polymeric structure shown in Fig. 1B. A crucial step for GNR formation is the CDH reaction. This step creates new C–C bonds, whereby the polymers planarize and form the (3,1) chiral ribbon structure (*20*). We found that CDH also produces an additional six-membered ring at the FeTPP-cGNR contact (shadowed ring in Fig. 1C), which improves the stability and the electronic conjugation of the connection. However, as we shall show here, the CDH reaction can also affect the porphyrin core by forming new five-membered rings (blue and red arrows in Fig. 1C), which fuse the pyrrole moieties to the graphenoid backbone and impose planarity to the tetrapyrrole core (*21*, *22*).

RESULTS

To produce FeTPP-cGNR hybrid systems, we first co-deposited small amounts of both DBBA and Br_4-FeTPP(Cl) species onto an atomically clean Au(111) surface and then activated the polymerization and CDH reactions by annealing the substrate (see Methods). The overview scanning tunneling microscopy (STM) image in Fig. 1D confirms that FeTPP fuses with cGNRs, as predefined by the position of the halogen substitution. For the case of a very small fraction of Br_4-FeTPP(Cl), we generally find well-formed cGNR segments connected to a single FeTPP fragment, in a varying number (numbers in Fig. 1D), and the absence of structures formed by several covalently connected FeTPP fragments (*19*). The prochiral character of the used cGNRs results in two enantiomeric structures on the surface (*10*) that lead to different angles between the arms of the contacted porphyrin. To resolve the precise structure of the atomic contacts between FeTPP and cGNRs, we used CO-terminated tips (*23*) and measured differential conductance (dI/dV) maps at constant height, in close proximity to the molecular hybrid. The presence of a CO molecule at the tip apex allows approaching the tip to the onset of repulsive Pauli forces, where the CO molecule transduces atomic-scale forces into changes of tunneling current with high resolution (*24*).

[1]CIC nanoGUNE, 20018 Donostia–San Sebastián, Spain. [2]Centro de Física de Materiales CFM/MPC (CSIC-UPV/EHU), 20018 Donostia–San Sebastián, Spain. [3]Donostia International Physics Center, 20018 Donostia–San Sebastián, Spain. [4]Centro Singular de Investigación en Química Biolóxica e Materiais Moleculares (CiQUS) and Departamento de Química Orgánica, Universidade de Santiago de Compostela, 15782 Santiago de Compostela, Spain. [5]Ikerbasque, Basque Foundation for Science, 48013 Bilbao, Spain.
*Corresponding author. Email: jli@nanogune.eu (J.L.); ji.pascual@nanogune.eu (J.I.P.)

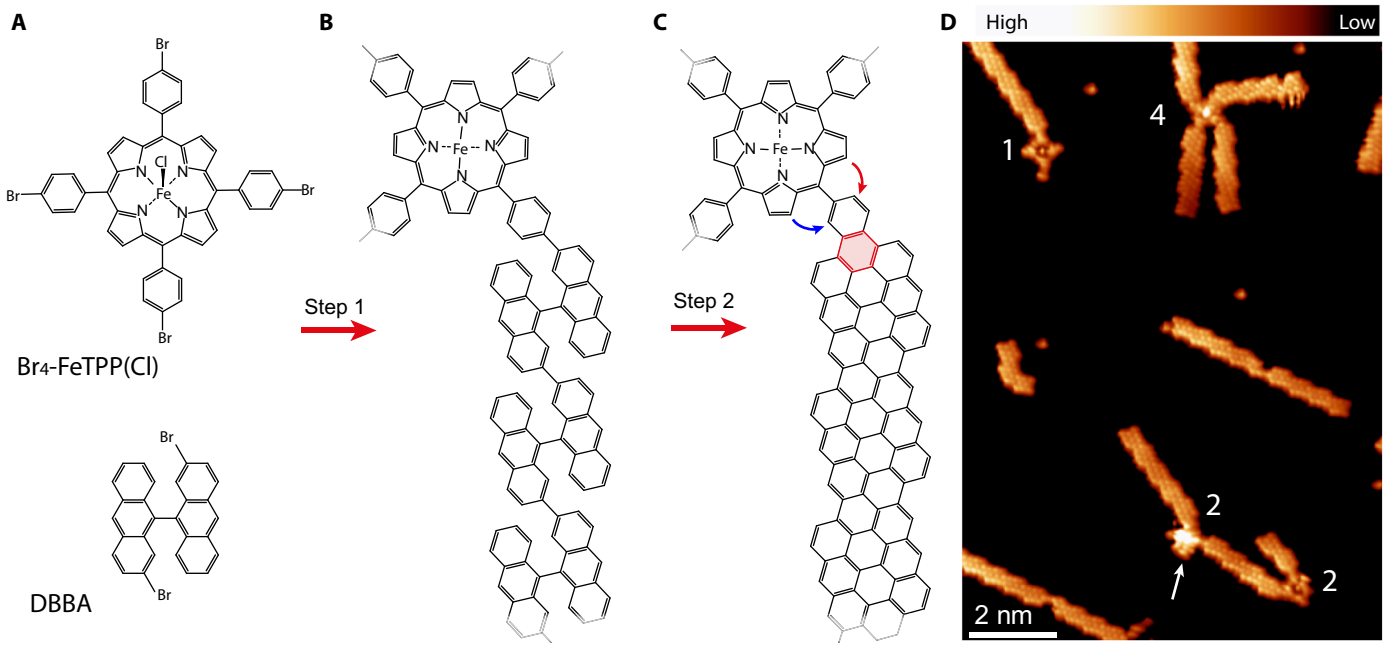

Fig. 1. Synthetic strategy to produce hybrid molecular systems composed of a magnetic FeTPP bonded to GNRs. (**A**) Structure of the monomers DBBA and Br_4-FeTPP(Cl) used for the on-surface reaction. DBBA is three-dimensional, appearing with two enantiomeric forms on the substrate. (**B**) Structure of a hybrid polymer of covalently linked monomers created after the Ullmann coupling step. At the annealing temperatures, the Cl ligand of the porphyrin is detached, whereas the DBBA molecule maintains its three-dimensional shape. (**C**) Structure of a molecular hybrid after the CDH step. The CDH reaction forms the new ring shadowed red in the image and can additionally fuse the porphyrin core in a clockwise (red arrow) or anticlockwise (blue arrow) manner to the contact phenyl. The fusion renders planar structures, in contrast to the known saddle shape of pristine FeTPP fragments. Note that two mirror-symmetric bonding configurations can form, depending on the chirality of the GNR. (**D**) High-resolution *dI/dV* image measured at constant height with a CO-terminated tip [$V_s = 5$ mV, $V_{ac} = 2$ mV root mean square (rms), and $R_t \sim 1$ gigaohm over pristine Au(111) regions], showing several molecular hybrids created on a Au(111) surface. Numbers quantify the GNRs connections to each of the four porphyrin centers of the image. The arrow points to an FeTPP moiety with a three-dimensional structure, whereas the other three on the image are planar.

Although most of the contacted FeTPP moieties are resolved as planar structures in the STM images, in a few cases (~5%), they appear as higher features (for example, the brighter FeTPP marked by an arrow in Fig. 1D). A close-up STM image of these higher molecules measured with a metallic tip (Fig. 2A) reproduces the well-known double-lobe structure caused by the saddle shape of the tetrapyrrole core on a surface (*16*, *25*).Therefore, these species correspond to intact FeTPP fragments that survive the on-surface reaction. The corresponding high-resolution image (Fig. 2B) shows instabilities caused by interactions of the CO tip with the nonplanar shape of the molecule. The image with a CO tip resolves, with high detail, the ring structure of the cGNR segments up to the connection to the FeTPP moieties, where new six-membered rings appear after the CDH step (as outlined in Fig. 1C).

Iron porphyrin species on gold surfaces preserve their magnetic moment and a large (easy-plane) magnetic anisotropy (*16*, *26*). To probe the survival of the FeTPP magnetic state after its contact to cGNRs, we measured the *dI/dV* spectra over different parts of the molecule. On the Fe center, spectra show a step-wise increase of conductance at symmetric bias values $V_s \approx \pm 7$ mV (Fig. 2C), with a characteristic asymmetric line shape. The position of the *dI/dV* steps and their shape reproduce tunneling spectra reported for pristine FeTPP on Au(111) (*16*) and thus can be interpreted as inelastic spin excitations of the $S = 1$ spin multiplet (see note S4). Spectra over the upper pyrrole groups (red pyrroles in Fig. 2A) show even more pronounced steps at the same excitation energy, also in agreement with the pristine case. Therefore, these plots demonstrate that the magnetic properties of the pristine FeTPP monomer, including its magnetic anisotropy energy (MAE), are preserved after they are fused to several cGNRs.

At the annealing temperatures required to activate the CDH (above 200°C), products (80% of the hybrids, for example, the other three FeTPP molecules in Fig. 1D) follow the reaction shown by arrows in Fig. 1C, resulting in pyrrole moieties fused to one of the two neighboring phenyl rings. The newly created five-membered rings impose a flat geometry to the tetrapyrrole core, which can have four possible configurations depending on the sequence of fusion, as described in fig. S1 (*22*).

Figure 3 (A to C) shows various examples of FeTPP species flattened with all pyrrole groups fused clockwise and with a different number of connecting ribbons. The high-resolution images unveil the ring structure of the contacts between cGNRs and flat-FeTPP, as depicted in the models shown in Fig. 3 (D to F). The four phenyl rings of the FeTPP unit now appear stable in the STM images and accompanied by the new five-membered rings shown as brighter features (compare the dashed rectangle in Fig. 3E). The alignment of this contact region with respect to the iron center unambiguously reveals the bonding orientation of the fused pyrroles.

We found that the magnetic properties of the Fe^{2+} ion survive the planarization process if a certain symmetry is maintained. In all cases where a C4 symmetry was adopted after CDH planarization (as in Fig. 3), the spectra over the iron center show *dI/dV* steps similar to those of the pristine compound, although with a slightly smaller bias onset ($V_s \sim \pm 5 \pm 1$ mV), reflecting a smaller MAE. The inelastic fingerprint appears independent of the number of connected cGNRs, providing evidence

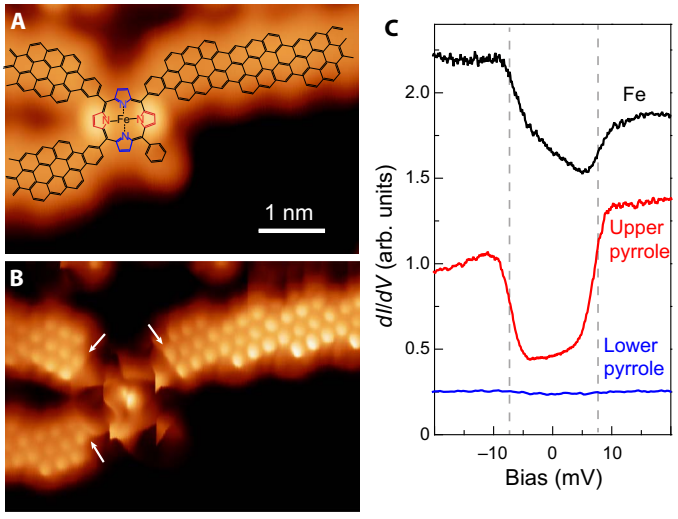

Fig. 2. Imaging and spectroscopy of intact FeTPP connected to cGNRs. (**A**) Constant current STM image (with a metal tip) of an FeTPP moiety connected to three cGNRs (V_s = 0.21 V and I_t = 16 pA). The corresponding structure (as in Fig. 1C) is superimposed. As in the study of Rubio-Verdú *et al.* (*16*), the intact FeTPP fragment has a saddle shape, with two lobes due to two pyrrole units pointing upward (red). (**B**) Constant height *dI/dV* map of the same structure as in (A) with CO-terminated tip (V_s = 0 mV, V_{ac} = 2 mV rms, and R_t ~ 1 gigaohm). Arrows point to new six-membered rings created after CDH step at the contact region. (**C**) *dI/dV* spectra taken on the central Fe atom, on the red pyrrole, and on the blue pyrrole (R_t ~ 50 megaohm on site and V_{ac} = 0.4 mV rms). arb. units, arbitrary units.

that their impact on the Fe center is negligible. The new structure of the tetrapyrrole ligand preserves the spin and its easy-plane anisotropy D because it maintains the original square-planar ligand field configuration around the Fe^{2+} ion. However, the planarization process causes a slight reduction of magnetic anisotropy, which is generally associated to the weakening of the ligand field around the Fe^{2+} ion (*26*). We speculate that this weakening might be caused by an in-plane distortion of the pyrrole units, pulled backward by the new C–C bonds in the flattened structures.

Two other configurations of flat-FeTPP moieties contacted to cGNRs are shown in Fig. 4. In the structure of Fig. 4A, the porphyrin core is fused clockwise to two of the contact phenyls and anticlockwise to the other two, displaying a mirror symmetry with axis indicated in the corresponding model in Fig. 4C. The structure of Fig. 4B presents the clockwise fusion of porphyrin core to three contact phenyl and anticlockwise fusion to one contact phenyl (Fig. 4D), disrupting the symmetry of the ligand field around the Fe^{2+} ion. The spectra over the center still appear with inelastic features but at lower bias values (V_s ~ ±3 ± 1 and ±2 ± 1 mV, for the spectra on Fig. 4, A and B, respectively), whereas in other structures, it can completely vanish (see fig. S3).

DISCUSSION

Figure 4F collects the average bias position of inelastic steps obtained from the spectra on a set of 20 FeTPP-cGNR hybrids, distributed according to the four configurations presented in Figs. 2 to 4. The

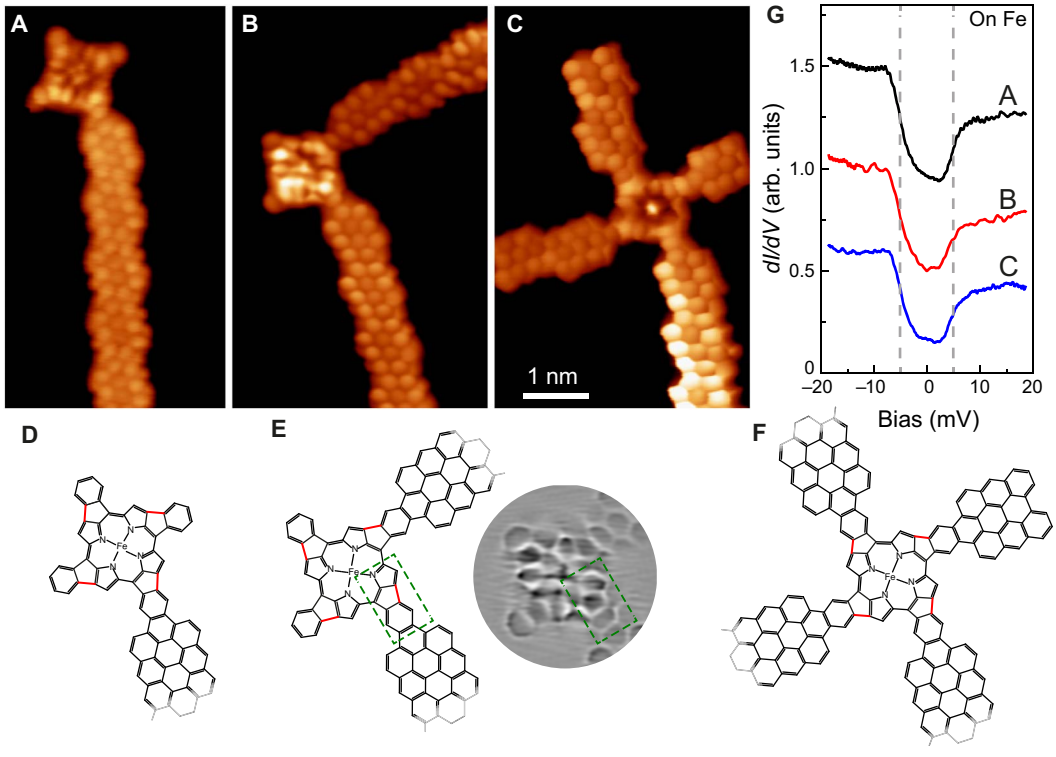

Fig. 3. Imaging and spectroscopy of contacted FeTPP fused with C4 symmetry. (**A** to **C**) Constant height *dI/dV* maps of planar FeTPP fused to one, two, and four cGNRs, respectively, measured with a CO-functionalized tip (V_s = 0 mV, V_{ac} = 2 mV rms, and R_t ~ 1 gigaohm). All images share the same scale bar. (**D** to **F**) Structures corresponding to the hybrids pictured in (A) to (C), respectively. Only a part of the models is shown here for clarity. The red bonds in the structures indicate the clockwise fusion of porphyrin core to the contact phenyl. The green dashed rectangular in(E) highlights the junction structure between FeTPP and cGNRs, with three rings easily recognized in the included Laplacian-filtered image of (B). (**G**) *dI/dV* spectra taken on the central Fe atoms of the structures in (A) to (C) (R_t ~ 50 megaohm on site and V_{ac} = 0.4 mV rms). The *dI/dV* spectra are vertically shifted for clarity.

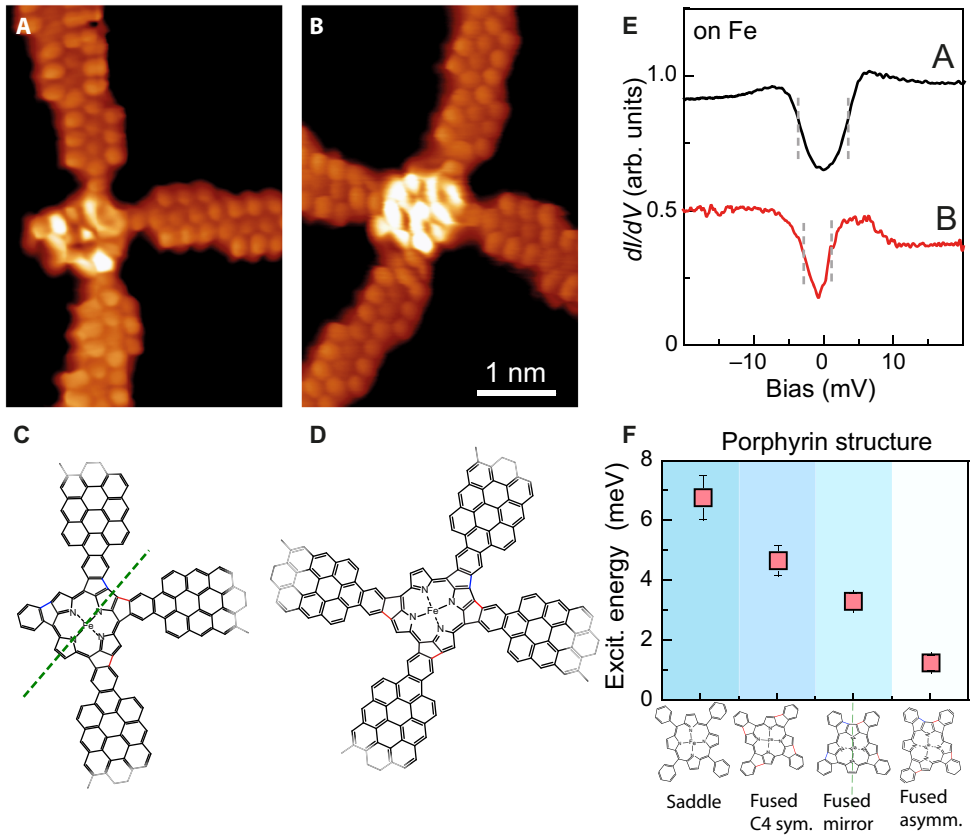

Fig. 4. Reduction of spin excitation energy with the symmetry of the fused FeTPP. (**A** and **B**) Constant height *dI/dV* maps with a CO tip of hybrid cGNR-FeTPP structures with flat porphyrin moieties, planarized following a mirror-symmetric sequence of fusion orientation or with no symmetry (sym.), respectively (V_s = 0 mV, V_{ac} = 2 mV rms, and R_t ~ 1 gigaohm). All images share the same scale bar. (**C** and **D**) Structures of the hybrids pictured in (A) and (B), respectively. Only a part of the models is shown here for clarity. The red and blue bonds in the structures indicate the creations of five-membered rings by the clockwise and anticlockwise fusion of porphyrin core to the contact phenyl, respectively. The green dashed line in (C) indicates the mirror plane of the structure. (**E**) *dI/dV* spectra taken on the central Fe atom of the structures in (A) and (B) (R_t ~ 50 megaohm on site and V_{ac} = 0.4 mV rms). The *dI/dV* spectra are vertically shifted for clarity. (**F**) Summary of spin excitation (Excit.) energy measured for the different contacted FeTPP structures studied here. The values represent the average extracted for a total of 20 systems studied in total (see figs. S1 and S2 for further information). asymm., asymmetric.

general trend confirms that the spin excitation energy decreases when the molecule planarizes and further decreases as the symmetry of the pyrrolic ligands is reduced. There are several processes that probably contribute to the reduction of the magnetic anisotropy of the molecular spin. As mentioned above, the MAE is very sensitive to the strength and the symmetry of the ligand field. In particular, the reduction of the axial symmetry inherently leads to a larger degree of orbital mixing, which reduces the magnetic anisotropy, in agreement with the observed trend (*27*, *28*). In addition, the stronger interaction of the flattened molecules with the surface might also lead to a MAE reduction. For example, sub-integer variations in charge occupancy, leading to valence fluctuations or simply exchange scattering with the surface, might cause a renormalization of the magnetic anisotropy even in the absence of Kondo effect (*29*, *30*).

The survival of the magnetic properties of the pristine component proves that cGNRs are ideal systems for contacting and accessing individual magnetic porphyrin molecules. However, the performance of GNR-based molecular systems relies on the premise that the electronic properties of the ribbons are not largely perturbed by the contact. The (3,1) GNRs used in this study are semiconductors with an energy bandgap of ~0.7 eV and show the absence of edge states due to their small width (*31*). Point spectra over porphyrin core and cGNR (Fig. 5A) show clear resonances at the energies of frontier molecular resonances and transport bands, respectively. Their electronic structure resemble closely that of the individual components (see note S4), confirming that their connection preserves their electronic properties. We note that, although the conduction and valence band of the cGNR overlap in energy with LUMO+1– and HOMO (highest occupied molecular orbital)–derived resonances of FeTPP, the state close to E_F in the porphyrin [the lowest unoccupied molecular orbital (LUMO); see note S4] matches the cGNR bandgap.

Figure 5 (D and E) shows two *dI/dV* maps of a cGNR-FeTPP hybrid measured at the onset energy of the cGNR frontier bands. As a reference, we show in Fig. 5 (B and C) the similar maps for a pristine ribbon (*31*). Both conduction and valence bands reproduce the shape of the cGNR density of states (DOS) precisely up to the contact region. There, a small depletion of DOS contrast is observed similar to that at the termini of pristine cGNRs (shown in the same image for comparison). Thus, the impact of a contact to a porphyrin can be regarded as negligible, and the cGNR electronic structure remains unaffected until its termination.

On-surface synthesis thus shows to be a viable strategy to incorporate functional molecules into a graphene-based device while maintaining its functionality. We foresee its useful application in incorporating other species relevant for molecular spintronics (*32*), optoelectronics (*17*), or catalysis (*33*) in the junction between GNRs, benefiting from the atomically precise control of a covalent and rigid contact structure.

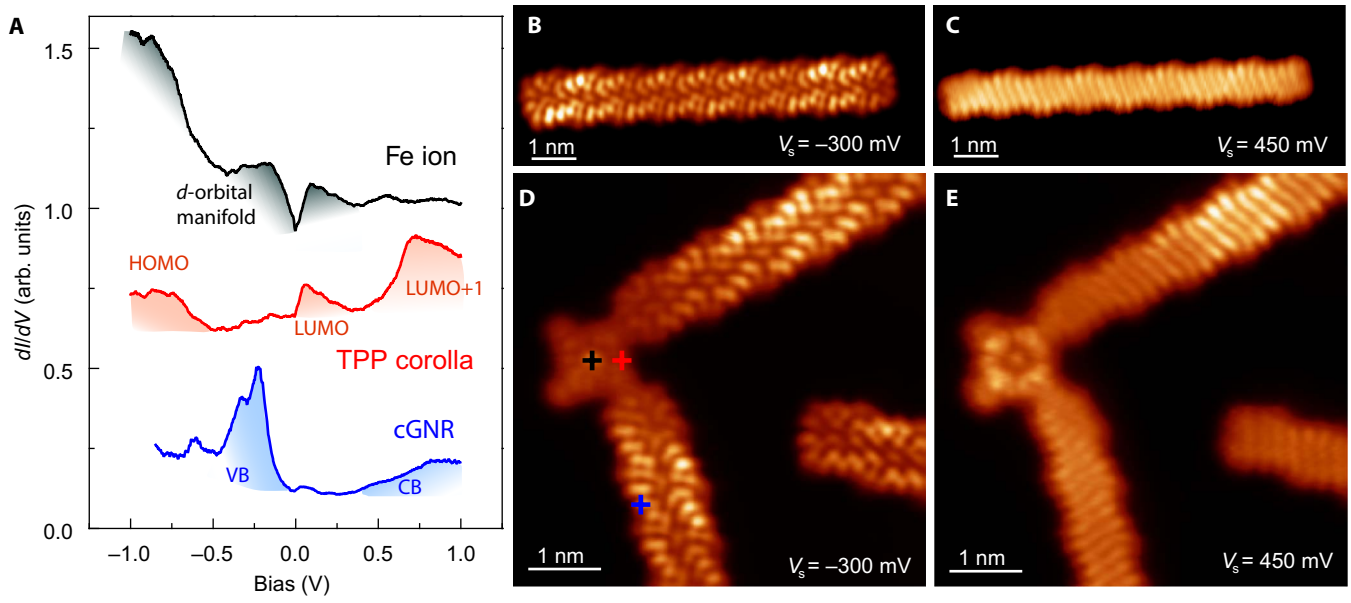

Fig. 5. Comparison of LDOS of pristine and contacted cGNRs. (**A**) *dI/dV* spectra on the center of a contacted porphyrin (top), over a pyrrole group (middle), and over the connected cGNR (bottom). The colored shadows mark relevant bands and resonances, as discussed in the Supplementary Materials and by Rubio-Verdú *et al.* (*16*). (**B** and **C**) Constant height *dI/dV* maps of a pristine cGNR measured at the onset values of valence and conduction bands, respectively (R_t ~ 5 gigaohm; the tip was functionalized with CO). (**D** and **E**) Constant height *dI/dV* maps of two cGNRs connected to a planar FeTPP (the structure shown in Fig. 3B) measured as in (A) and (B) at the onset of valence band (VB) and conduction band (CB), respectively. The brighter segment in the upper cGNR branch is caused by the Au(111) herringbone reconstruction underneath.

METHODS

All these experiments were performed in a custom-made low-temperature STM, at low temperatures (5 K), and under ultrahigh vacuum (UHV) conditions. The Au(111) substrate was cleaned in UHV by repeated cycles of Ne^+ ion sputtering and subsequent annealing at 730 K. The two molecular building blocks DBBA [prepared as described by de Oteyza *et al.* (*10*)] and Br_4-FeTPP(Cl) (Porphyrin Systems GmbH) were co-deposited on the Au(111) surface at room temperature by thermal sublimation from quartz crucibles (sublimation temperatures, T_{DBBA} = 160°C and $T_{Br_4\text{-FeTPP(Cl)}}$ = 300°C). The sample was then heated to 200°C for 10 min to activate the polymerization and to 250°C for 5 min to complete the CDH reaction. A tungsten tip functionalized with a CO molecule was used for imaging and spectroscopy. The high-resolution *dI/dV* images were acquired in constant height mode, at very small voltages, and junction resistances of typically 20 megaohm. *dI/dV* signals were recorded using a lock-in amplifier with a bias modulation of V_{rms} = 0.4 mV at 760 Hz. The presence of a CO molecule on the tip did not affect the measured spectra, as we could check by comparing the results with metallic tips. In particular, frustrated translational modes of the CO molecule were absent in most of our spectra, probably hidden by the much larger inelastic signal due to spin excitation. Analysis of STM data was performed with the WSxM software (*34*).

SUPPLEMENTARY MATERIALS

Supplementary material for this article is available at http://advances.sciencemag.org/cgi/content/full/4/2/eaaq0582/DC1

note S1. Symmetry of fused FeTPP moieties
note S2. Spectra on pyrrole subunits of GNR-contacted FeTPPs
note S3. Anomalous contacts between FeTPP and GNRs
note S4. Electronic structure of contacted FeTPPs
fig. S1. Statistics of different types of FeTPP connected to cGNRs.
fig. S2. *dI/dV* spectra taken over the pyrrole subunits of cGNR-contacted FeTPP moieties.
fig. S3. Additional bond formation between planar FeTPP and cGNRs.
fig. S4. Comparison of wide-range *dI/dV* spectra on pristine and on contacted FeTPP.
fig. S5. Frontier orbitals of FeTPP and their localization in the macrocycle.

REFERENCES AND NOTES

1. E. Lörtscher, Wiring molecules into circuits. *Nat. Nanotechnol.* **8**, 381–384 (2013).
2. F. Prins, A. Barreiro, J. W. Ruitenberg, J. S. Seldenthuis, N. Aliaga-Alcalde, L. M. K. Vandersypen, H. S. J. van der Zant, Room-temperature gating of molecular junctions using few-layer graphene nanogap electrodes. *Nano Lett.* **11**, 4607–4611 (2011).
3. J. A. Mol, C. S. Lau, W. J. M. Lewis, H. Sadeghi, C. Roche, A. Cnossen, J. H. Warner, C. J. Lambert, H. L. Anderson, G. A. D. Briggs, Graphene-porphyrin single-molecule transistors. *Nanoscale* **7**, 13181–13185 (2015).
4. C. Jia, A. Migliore, N. Xin, S. Huang, J. Wang, Q. Yang, S. Wang, H. Chen, D. Wang, B. Feng, Z. Liu, G. Zhang, D.-H. Qu, H. Tian, M. A. Ratner, H. Q. Xu, A. Nitzan, X. Guo, Covalently bonded single-molecule junctions with stable and reversible photoswitched conductivity. *Science* **352**, 1443–1445 (2016).
5. S. Zhang, S. Tang, J. Lei, H. Dong, H. Ju, Functionalization of graphene nanoribbons with porphyrin for electrocatalysis and amperometric biosensing. *J. Electroanal. Chem.* **656**, 285–288 (2011).
6. Y. Cao, S. Dong, S. Liu, L. He, L. Gan, X. Yu, M. L. Steigerwald, X. Wu, Z. Liu, X. Guo, Building high-throughput molecular junctions using indented graphene point contacts. *Angew. Chem. Int. Ed. Engl.* **51**, 12228–12232 (2012).
7. Y. He, M. Garnica, F. Bischoff, J. Ducke, M.-L. Bocquet, M. Batzill, W. Auwärter, J. V. Barth, Fusing tetrapyrroles to graphene edges by surface-assisted covalent coupling. *Nat. Chem.* **9**, 33–38 (2017).
8. J. Cai, P. Ruffieux, R. Jaafar, M. Bieri, T. Braun, S. Blankenburg, M. Muoth, A. P. Seitsonen, M. Saleh, X. Feng, K. Müllen, R. Fasel, Atomically precise bottom-up fabrication of graphene nanoribbons. *Nature* **466**, 470–473 (2010).
9. P. Ruffieux, S. Wang, B. Yang, C. Sánchez-Sánchez, J. Liu, T. Dienel, L. Talirz, P. Shinde, C. A. Pignedoli, D. Passerone, T. Dumslaff, X. Feng, K. Müllen, R. Fasel, On-surface synthesis of graphene nanoribbons with zigzag edge topology. *Nature* **531**, 489–492 (2016).
10. D. G. de Oteyza, A. García-Lekue, M. Vilas-Varela, N. Merino-Díez, E. Carbonell-Sanromà, M. Corso, G. Vasseur, C. Rogero, E. Guitián, J. I. Pascual, J. E. Ortega, Y. Wakayama, D. Peña, Substrate-independent growth of atomically precise chiral graphene nanoribbons. *ACS Nano* **10**, 9000–9008 (2016).

11. J. Hieulle, E. Carbonell-Sanromà, M. Vilas-Varela, A. Garcia-Lekue, E. Guitián, D. Peña, J. I. Pascual, On-surface route for producing planar nanographenes with azulene moieties. *Nano Lett.* **18**, 418–423 (2018).
12. J. Cai, C. A. Pignedoli, L. Talirz, P. Ruffieux, H. Söde, L. Liang, V. Meunier, R. Berger, R. Li, X. Feng, K. Müllen, R. Fasel, Graphene nanoribbon heterojunctions. *Nat. Nanotechnol.* **9**, 896–900 (2014).
13. Y.-C. Chen, T. Cao, C. Chen, Z. Pedramrazi, D. Haberer, D. G. de Oteyza, F. R. Fischer, S. G. Louie, M. F. Crommie, Molecular bandgap engineering of bottom-up synthesized graphene nanoribbon heterojunctions. *Nat. Nanotechnol.* **10**, 156–160 (2015).
14. E. Carbonell-Sanromà, P. Brandimarte, R. Balog, M. Corso, S. Kawai, A. Garcia-Lekue, S. Saito, S. Yamaguchi, E. Meyer, D. Sánchez-Portal, J. I. Pascual, Quantum dots embedded in graphene nanoribbons by chemical substitution. *Nano Lett.* **17**, 50–56 (2017).
15. B. W. Heinrich, G. Ahmadi, V. L. Müller, L. Braun, J. I. Pascual, K. J. Franke, Change of the magnetic coupling of a metal–organic complex with the substrate by a stepwise ligand reaction. *Nano Lett.* **13**, 4840–4843 (2013).
16. C. Rubio-Verdú, A. Sarasola, D.-J. Choi, Z. Majzik, R. Ebeling, M. R. Calvo, M. M. Ugeda, A. García-Lekue, D. Sánchez-Portal, J. I. Pascual, Orbital-selective spin excitation of a magnetic porphyrin. https://arxiv.org/abs/1708.01268 (2017).
17. M. C. Chong, G. Reecht, H. Bulou, A. Boeglin, F. Scheurer, F. Mathevet, G. Schull, Narrow-line single-molecule transducer between electronic circuits and surface plasmons. *Phys. Rev. Lett.* **116**, 036802 (2016).
18. T. G. Gopakumar, H. Tang, J. Morillo, R. Berndt, Transfer of Cl ligands between adsorbed iron tetraphenylporphyrin molecules. *J. Am. Chem. Soc.* **134**, 11844–11847 (2012).
19. L. Grill, M. Dyer, L. Lafferentz, M. Persson, M. V. Peters, S. Hecht, Nano-architectures by covalent assembly of molecular building blocks. *Nat. Nanotechnol.* **2**, 687–691 (2007).
20. M. Treier, C. A. Pignedoli, T. Laino, R. Rieger, K. Müllen, D. Passerone, R. Fasel, Surface-assisted cyclodehydrogenation provides a synthetic route towards easily processable and chemically tailored nanographenes. *Nat. Chem.* **3**, 61–67 (2011).
21. M. Röckert, M. Franke, Q. Tariq, S. Ditze, M. Stark, P. Uffinger, D. Wechsler, U. Singh, J. Xiao, H. Marbach, H.-P. Steinrück, O. Lytken, Coverage- and temperature-dependent metalation and dehydrogenation of tetraphenylporphyrin on Cu(111). *Chemistry* **20**, 8948–8953 (2014).
22. A. Wiengarten, J. A. Lloyd, K. Seufert, J. Reichert, W. Auwärter, R. Han, D. A. Duncan, F. Allegretti, S. Fischer, S. C. Oh, Ö. Sağlam, L. Jiang, S. Vijayaraghavan, D. Écija, A. C. Papageorgiou, J. V. Barth, Surface-assisted cyclodehydrogenation; break the symmetry, enhance the selectivity. *Chemistry* **21**, 12285–12290 (2015).
23. L. Gross, F. Mohn, N. Moll, P. Liljeroth, G. Meyer, The chemical structure of a molecule resolved by atomic force microscopy. *Science* **325**, 1110–1114 (2009).
24. O. Krejčí, P. Hapala, M. Ondráček, P. Jelínek, Principles and simulations of high-resolution STM imaging with a flexible tip apex. *Phys. Rev. B* **95**, 045407 (2017).
25. W. Auwärter, D. Écija, F. Klappenberger, J. V. Barth, Porphyrins at interfaces. *Nat. Chem.* **7**, 105–120 (2015).
26. B. W. Heinrich, L. Braun, J. I. Pascual, K. J. Franke, Tuning the magnetic anisotropy of single molecules. *Nano Lett.* **15**, 4024–4028 (2015).
27. J. J. Parks, A. R. Champagne, T. A. Costi, W. W. Shum, A. N. Pasupathy, E. Neuscamman, S. Flores-Torres, P. S. Cornaglia, A. A. Aligia, C. A. Balseiro, G. K.-L. Chan, H. D. Abruña, D. C. Ralph, Mechanical control of spin states in spin-1 molecules and the underscreened Kondo effect. *Science* **328**, 1370–1373 (2010).
28. B. Bryant, A. Spinelli, J. J. T. Wagenaar, M. Gerrits, A. F. Otte, Local control of single atom magnetocrystalline anisotropy. *Phys. Rev. Lett.* **111**, 127203 (2013).
29. J. C. Oberg, M. R. Calvo, F. Delgado, M. Moro-Lagares, D. Serrate, D. Jacob, J. Fernández-Rossier, C. F. Hirjibehedin, Control of single-spin magnetic anisotropy by exchange coupling. *Nat. Nanotechnol.* **9**, 64–68 (2014).
30. D. Jacob, Renormalization of single-ion magnetic anisotropy in the absence of Kondo effect. https://arxiv.org/abs/1712.01005 (2017).
31. N. Merino-Díez, J. Li, A. Garcia-Lekue, G. Vasseur, M. Vilas-Varela, E. Carbonell-Sanromà, M. Corso, J. Enrique Ortega, D. Peña, J. I. Pascual, D. G. de Oteyza, Unraveling the electronic structure of narrow atomically-precise chiral graphene nanoribbons. *J. Phys. Chem. Lett.* **9**, 25–30 (2018).
32. L. Bogani, W. Wernsdorfer, Molecular spintronics using single-molecule magnets. *Nat. Mater.* **7**, 179–186 (2008).
33. D. Deng, X. Chen, L. Yu, X. Wu, Q. Liu, Y. Liu, H. Yang, H. Tian, Y. Hu, P. Du, R. Si, J. Wang, X. Cui, H. Li, J. Xiao, T. Xu, J. Deng, F. Yang, P. N. Duchesne, P. Zhang, J. Zhou, L. Sun, J. Li, X. Pan, X. Bao, A single iron site confined in a graphene matrix for the catalytic oxidation of benzene at room temperature. *Sci. Adv.* **1**, e1500462 (2015).
34. I. Horcas, R. Fernández, J. M. Gómez-Rodríguez, J. Colchero, J. Gómez-Herrero, A. M. Baro, WSXM: A software for scanning probe microscopy and a tool for nanotechnology. *Rev. Sci. Instrum.* **78**, 013705 (2007).

Acknowledgments: We thank C. Rúbio-Verdú, A. G. Lekue, A. Sarasola, and D. Sánchez Portal for the fruitful discussions regarding the magnetic state of FeTPP and the electronic structure of cGNRs. **Funding:** We acknowledge the financial support from Spanish Agencia Estatal de Investigación (AEI) (project nos. MAT2016-78293-C6 and FIS2015-62538-ERC, and the Maria de Maeztu Units of Excellence Programme MDM-2016-0618), the Basque Government (Department Industry, grant no. PI-2015-1-42), the European project PAMS (610446), the Xunta de Galicia (Centro singular de investigación de Galicia accreditation 2016 to 2019, ED431G/09), the European Research Council (grant agreement no. 635919), and the European Regional Development Fund. **Author contributions:** J.L., E.C.-S., and J.I.P. devised the experiment. M.V.-V. and D.P. did the organic synthesis of the cGNR molecular precursor. J.L. and N.M.-D. realized the measurements. All authors discussed the results. J.L. and J.I.P. wrote the manuscript with the support of all the authors. **Competing interests:** The authors declare that they have no competing interests. **Data and materials availability:** All data needed to evaluate the conclusions in the paper are present in the paper and/or the Supplementary Materials. Additional data related to this paper may be requested from the authors. The Supplementary Materials available include (i) statistics on the fused FeTPP moieties, (ii) inelastic spectra on pyrrole subunits of GNR-contacted FeTPPs, (iii) anomalous connections between FeTPP and GNRs, and (iv) electronic structure of contacted FeTPPs.

Submitted 27 September 2017
Accepted 16 January 2018
Published 16 February 2018
10.1126/sciadv.aaq0582

Citation: J. Li, N. Merino-Díez, E. Carbonell-Sanromà, M. Vilas-Varela, D. G. de Oteyza, D. Peña, M. Corso, J. I. Pascual, Survival of spin state in magnetic porphyrins contacted by graphene nanoribbons. *Sci. Adv.* **4**, eaaq0582 (2018).

Science Advances

Survival of spin state in magnetic porphyrins contacted by graphene nanoribbons

Jingcheng Li, Nestor Merino-Díez, Eduard Carbonell-Sanromà, Manuel Vilas-Varela, Dimas G. de Oteyza, Diego Peña, Martina Corso and Jose Ignacio Pascual

Sci Adv **4** (2), eaaq0582.
DOI: 10.1126/sciadv.aaq0582